This article was downloaded by: [Siauliu University Library]
On: 17 February 2013, At: 06:59
Publisher: Taylor & Francis
Informa Ltd Registered in England and Wales Registered Number: 1072954 Registered office: Mortimer House, 37-41 Mortimer Street, London W1T 3JH, UK

Advanced Composite Materials
Publication details, including instructions for authors and subscription information:
http://www.tandfonline.com/loi/tacm20

Numerical simulation of the pressure infiltration of fibrous preforms during MMC processing

Chih-Yuan Chang

Version of record first published: 02 Apr 2012.

To cite this article: Chih-Yuan Chang (2006): Numerical simulation of the pressure infiltration of fibrous preforms during MMC processing, Advanced Composite Materials, 15:3, 287-300

To link to this article: http://dx.doi.org/10.1163/156855106778392070

PLEASE SCROLL DOWN FOR ARTICLE

Full terms and conditions of use: http://www.tandfonline.com/page/terms-and-conditions

This article may be used for research, teaching, and private study purposes. Any substantial or systematic reproduction, redistribution, reselling, loan, sub-licensing, systematic supply, or distribution in any form to anyone is expressly forbidden.

The publisher does not give any warranty express or implied or make any representation that the contents will be complete or accurate or up to date. The accuracy of any instructions, formulae, and drug doses should be independently verified with primary sources. The publisher shall not be liable for any loss, actions, claims, proceedings, demand, or costs or damages whatsoever or howsoever caused arising directly or indirectly in connection with or arising out of the use of this material.

Adv. Composite Mater., Vol. 15, No. 3, pp. 287–300 (2006)
© VSP 2006.
Also available online - www.brill.nl/acm

Downloaded by [Siauliu University Library] at 06:59 17 February 2013

Numerical simulation of the pressure infiltration of fibrous preforms during MMC processing *

CHIH-YUAN CHANG †

Department of Automation Engineering, Kao Yuan University, 1821 Chung-Shan Road, Lu-Chu, Kaohsiung, Taiwan 82101, Republic of China

Received 9 May 2005; accepted 8 August 2005

Abstract—In the pressure infiltration process of metal-matrix composites, molten metal is injected under external pressure into a porous preform of the reinforcing phase and solidified, either during infiltration or after the mold is filled. To simplify the problem, the assumption of isothermally saturated fibrous preform with molten metal is adopted. The flow of molten metal is a moving boundary phenomenon which is similar to a fluid flowing through a porous medium. A numerical technique, body-fitted finite element method (FEM), is used to generate grids inside the physical domain and to calculate the distribution of pressure and other relative properties. Results show that the injection flow rate exponentially decreases with the infiltration time. Increasing injection pressure can effectively reduce the infiltration time. A simple and practical prediction of infiltration time under the various parameters is also provided in this study.

Keywords: Metal matrix composite; infiltration process; body-fitted finite element method.

NOMENCLATURE

f	fiber volume fraction
K	permeability (m^2)
P	pressure (Pa)
P_{inj}	injection pressure (Pa)
Re	Reynolds number
r_f	the radius of the flow front (m)
r_i	the radius of the inlet gate (m)

*Edited by the JSCM.

†E-mail: yuan@cc.kyu.edu.tw

u, v	velocity components in x, y direction (m/s)
v_c	contacting velocity (m/s)
v_r	radial fluid velocity (m/s)
W	mold width (m)
x, y	coordinate components in the physical domain (m)

Greek

ξ, η	coordinate components in the computational domain
Φ	shape function
Ω, Ψ	control functions in the body-fitted method
ρ	molten metal density (kg/m^3)
μ	molten metal viscosity (kg/(m s))
τ	time increment (s)

Downloaded by [Siauliu University Library] at 06:59 17 February 2013

1. INTRODUCTION

The advantages of fiber-reinforced metal-matrix composites (MMCs), such as their high specific stiffness, wear resistance and high temperature performance, have been known for many years; but the high cost of manufacturing near-net shape MMCs and fabrication difficulties have been major reasons for limiting their commercial application.

The fabrication techniques for MMCs depend very much upon the choice of fiber and matrix [1]. In recent years, several low-cost manufacturing techniques for MMCs have been developed based on casting technologies, such as squeeze/die casting, compo-casting and continuous casting. Among these fabrication methods, the pressure-casting technique appears to be effective in that it offers an improvement in wettability and the elimination of porosity due to solidification under pressure. Therefore, the pressure-casting technique seems to be most suitable to obtain economic parts of near-net shape MMCs. However, the phenomena governing infiltration are complex. A number of physical, mechanical, and chemical phenomena interact, including flow of liquid metal in a porous medium, heat and mass transfer related to metal solidification and chemical interfacial reactions between the reinforcement and matrix. These phenomena have been addressed over the past twenty years and several are now rather well identified [2–9]. Analytical and numerical solutions have been given and compared to experimental data, for unidirectional infiltration under constant applied pressure, including non-isothermal infiltration by a pure metal or by a binary alloy [6, 10]; for non-isothermal infiltration by a pure metal, taking into account the influence of preform deformability [11, 12]; and for isothermal infiltration, taking into account the influence of capillary phenomena [7]. For all these cases, the boundary condition of constant applied pressure and the unidirectional configuration allowed the use of a single combined variable to describe

time and position, thus yielding an analytical solution of the coupled phenomena. By using the one-dimensional solution, Aboulfatah *et al*. [13] proposed an experimental procedure to measure the mobility of the molten metal through the fibrous preform as a function of the volume fraction of solidified metal. Xia *et al*. [14] also proposed an approximate analytical solution for unidirectional saturated flow under a linearly increasing pressure function.

More general cases have been treated as well. In these, analytical solutions can no longer be derived, and numerical tools such as finite-element and finite-difference methods are applied. Lacoste *et al*. [15] presented a model for the infiltration of aluminum into a preform. A one-dimensional model was compared with existing analytical solutions and solved as well. The solutions, however, show that two-dimensional patterns would be restricted to the vicinity of the solidification front for the operating conditions analyzed. Tong and Khan [16] developed a numerical finite-difference model: the mold walls are insulated; only heat exchange between fibers and metal are taken into account. Recently, Biswas *et al*. [17] proposed a phenomenology model to describe fluid flow and transport phenomena for the case of unidirectional infiltration. From a finite elements model initially developed in hydrogeology, Dopler *et al*. [18] carried out a numerical simulation of the metal infiltration of a rigid fibrous preform with isothermal and low constant pressure. They could thereby follow the evolution of saturation according to the impregnation depth of the preform.

The aim of this study is to carry out an investigation for liquid metal flowing through fibrous preform in MMC processing to understand the flow phenomena under various conditions. The flow behavior of the infiltration process is considered two-dimensional in the present study. A numerical technique, based on the body-fitted FEM, is developed to solve the transient and irregular physical domains. Predictions of the changes in physical properties and the flow front of the molten metal are attempted. Furthermore, the limitation of the time increment for the quasi-steady-sate process is also discussed. Through this study more detailed knowledge of flow behavior in MMC process will be expected.

Downloaded by [Siauliu University Library] at 06:59 17 February 2013

2. NUMERICAL MODEL

The schematic diagram of the apparatus used in the pressure-casting process for MMCs fabrication is shown in Fig. 1. The model assumes a two-dimensional description of MMCs fabrication during the infiltration process, since the dimension of the mold thickness is much smaller than the dimensions in the planar direction. The size of the mold cavity is 0.25 m $\times$ 0.15 m $\times$ 0.005 m. A domain is symmetric for the x- and y-axes, so only one-quarter of the mold cavity needs to be considered in the numerical simulation, as shown in Fig. 2. The fibrous preform inside the mold cavity is assumed to be a porous medium. The infiltration process in MMCs can be regarded as a series of quasi-steady-state processes of molten metal flowing

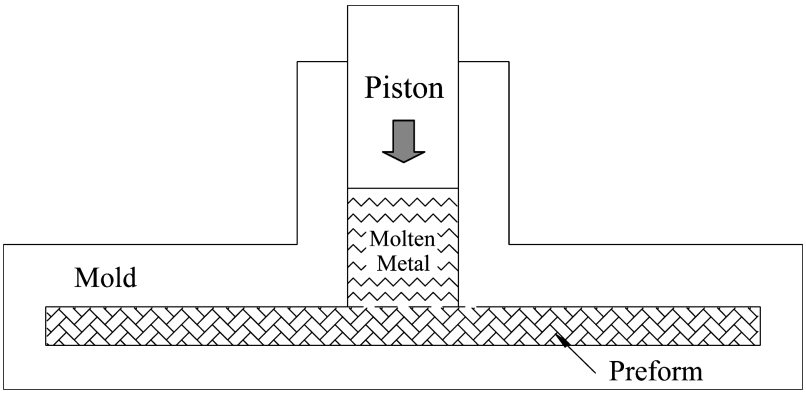

Figure 1. The schematic diagram of the apparatus in the die-casting process.

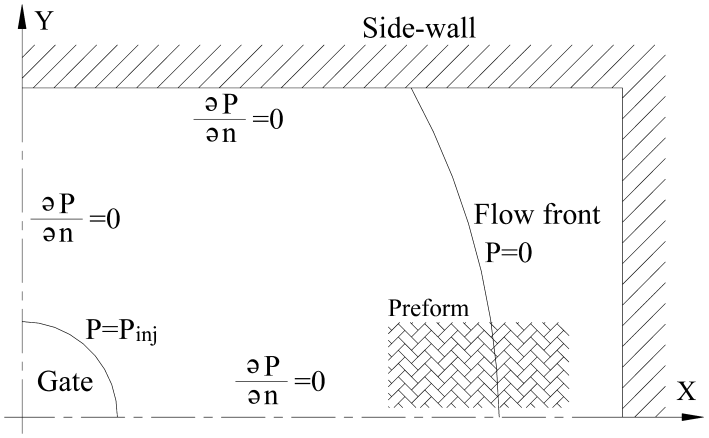

Figure 2. Boundary conditions.

through a porous medium. For simplification, several assumptions are made as follows.

(1) The fibrous preform is isotropic.
(2) The initial temperature of fibrous preform is equal that of molten metal so there is no heat-exchange between molten metal and fiber.
(3) The viscous dissipation is negligible.
(4) The inertial force is negligible compared to the viscous force because $Re \ll 1$.

Under the above assumptions, the momentum equation based on Darcy's law can be written in a two-dimensional form

$$u = -\frac{K_x}{(1-f)\mu}\frac{\partial P}{\partial x}, \tag{1a}$$

$$v = -\frac{K_y}{(1-f)\mu}\frac{\partial P}{\partial y}, \tag{1b}$$

Downloaded by [Siauliu University Library] at 06:59 17 February 2013

where K is the permeability of the fibrous preform, μ is the viscosity of molten metal and f is the fiber volume fraction. The conservation of mass is

$$\frac{\partial u}{\partial x} + \frac{\partial v}{\partial y} = 0. \tag{2}$$

The governing equation can then be deduced by combination of equations (1) and (2) as

$$\frac{\partial}{\partial x}\left(-\frac{K_x}{(1-f)\mu}\frac{\partial P}{\partial x}\right) + \frac{\partial}{\partial y}\left(-\frac{K_y}{(1-f)\mu}\frac{\partial P}{\partial y}\right) = 0. \tag{3}$$

Since the fibrous preform is isotropic, i.e. K_x is equal to K_y, equation (3) is further reduced to

$$\frac{\partial^2 P}{\partial x^2} + \frac{\partial^2 P}{\partial y^2} = 0. \tag{4}$$

The corresponding boundary conditions applicable to equation (4), as shown in Fig. 2, are

$$P = P_{\text{inj}}\ (\text{time}) \qquad \text{at the inlet gate,} \tag{5a}$$

$$\frac{\partial P}{\partial n} = 0 \qquad \text{along the } x,\ y\text{-axis and side-wall,} \tag{5b}$$

$$P = 0 \qquad \text{along the flow front.} \tag{5c}$$

Equation (5a) represents the inlet condition at the entrance. The injection pressure is a function of infiltration time. Equation (5b) interprets a symmetric condition along the x- and y-axes or no fluid flowing through the side wall. The gauge pressure is adopted so the pressure of the flow front is null in equation (5c).

3. NUMERICAL PROCEDURE

One of the difficulties of simulating the infiltration process is the numerical treatment of the moving, irregular front surface of the molten metal. The body-fitted FEM [19], the combination of body-fitted grid generation with the FEM, provides numerous advantages, such as uniformly spaced grids, easy application of surface boundary conditions and modular technique, etc. It is well suited to solve the free moving boundary problem.

3.1. Galerkin's method

In the present FEM model, the method of weight residual adopts the Galerkin method. Galerkin's residual equation for governing equation (4) can be derived

Downloaded by [Siauliu University Library] at 06:59 17 February 2013

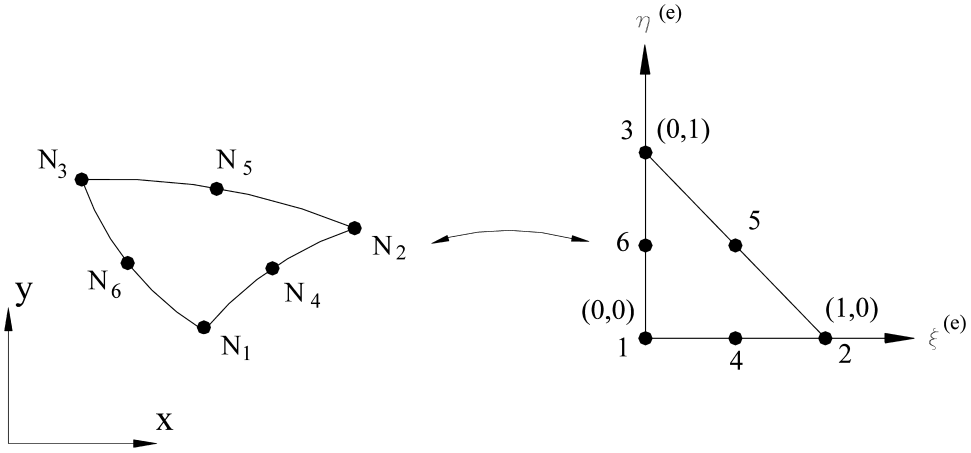

Figure 3. A 2D, 6-nodal quadratic isoparametrical triangular element.

from

$$\int^{(e)} \int \left(\frac{\partial^2 P}{\partial x^2} + \frac{\partial^2 P}{\partial y^2} \right) \Phi_j \, \mathrm{d}x \, \mathrm{d}y = 0, \quad j = 1, 2, \ldots, 6, \tag{6}$$

where Φ_j is the shape function or trial function [20]. The element type applied in the present simulation is a 2D, 6-nodal quadratic isoparametrical triangular element, shown in Fig. 3. The corresponding shape functions are

$$\begin{aligned}
\Phi_1(\xi, \eta) &= (1 - (\xi + \eta))(1 - 2(\xi + \eta)), \\
\Phi_2(\xi, \eta) &= \xi(2\xi - 1), \\
\Phi_3(\xi, \eta) &= \eta(2\eta - 1), \\
\Phi_4(\xi, \eta) &= 4\xi(1 - (\xi + \eta)), \\
\Phi_5(\xi, \eta) &= 4\xi\eta, \\
\Phi_6(\xi, \eta) &= 4\eta(1 - (\xi + \eta)),
\end{aligned} \tag{7}$$

where ξ and η are the local coordinates for each element. Integrating equation (6) by parts once and applying boundary conditions into the equation, the pressure distribution can be calculated numerically.

3.2. Nodal coordinates

The nodal coordinates of the present FEM scheme are generated by the body-fitted method [21]. A set of elliptic partial differential equations is used as follows.

$$\xi_{xx} + \xi_{yy} = \Omega(\xi, \eta)(\xi_x^2 + \xi_y^2), \tag{8a}$$

$$\eta_{xx} + \eta_{yy} = \Psi(\xi, \eta)(\eta_x^2 + \eta_y^2), \tag{8b}$$

Downloaded by [Siauliu University Library] at 06:59 17 February 2013

where Ω and Ψ are the control functions. Interchanging the dependent variables (ξ, η) with the independent variables (x, y) in the above equations yields

$$a(x_{\xi\xi} + \Omega x_\xi) - 2bx_{\xi\eta} + c(x_{\eta\eta} + \Psi x_\eta) = 0, \tag{9a}$$

$$a(y_{\xi\xi} + \Omega y_\xi) - 2by_{\xi\eta} + c(y_{\eta\eta} + \Psi y_\eta) = 0, \tag{9b}$$

where $a = x_\eta^2 + y_\eta^2$, $b = x_\xi x_\eta + y_\xi y_\eta$ and $c = x_\xi^2 + y_\xi^2$: ξ and η are taken as coordinates in the computational domain. Based on the assumptions that the curvature along the geometric boundaries is locally zero and the grid lines are orthogonal to each other in the vicinity of geometric boundaries, the control functions are determined by

$$\Omega = -(x_{\xi\xi}x_\xi + y_{\xi\xi}y_\xi)/(x_\xi^2 + y_\xi^2), \tag{10a}$$

$$\Psi = -(x_{\eta\eta}x_\eta + y_{\eta\eta}y_\eta)/(x_\eta^2 + y_\eta^2), \tag{10b}$$

along the geometric boundaries. For the interior points, the control function is interpolated from that on the geometric boundaries. The form of equations (9) in finite difference method (FDM) is

$$\begin{aligned} &a(R_{i+1,j} - 2R_{i,j} + R_{i-1,j} + \Omega(R_{i+1,j} - R_{i-1,j})/2) \\ &\quad - 2b(R_{i+1,j+1} - R_{i-1,j+1} + R_{i+1,j-1} + R_{i-1,j-1})/4 \\ &\quad + c(R_{i,j+1} - 2R_{i,j} + R_{i-1,j} + \Psi(R_{i,j+1} - R_{i,j-1})/2) = 0, \end{aligned} \tag{11}$$

where R can be x or y. The moving mesh techniques are adopted in the present paper. The techniques can achieve a better accuracy of the free surface. Thus, the nodal coordinates are updated for each time step. For the purpose of saving computational space and time, the number of elements is proportional to the volume of filled liquid. Certainly, a transformation of numbering of nodes between the body-fitted FDM and FEM is necessary in the pre-process of the FEM. Figure 4 illustrate the transformation mapping. Thus the body-fitted FEM is an auto-meshed scheme. The details of the numerical procedure are described by the flow chart as shown in Fig. 5.

4. RESULTS AND DISCUSSION

In the present study, Wood alloy (50% Bi, 25% Pb, 12.5% Cd, and 12.5% Sn) is used for the numerical test. The solidification temperature of Wood alloy is 70°C and, because it is close to a eutectic composition with an invariant solidification

Downloaded by [Siauliu University Library] at 06:59 17 February 2013

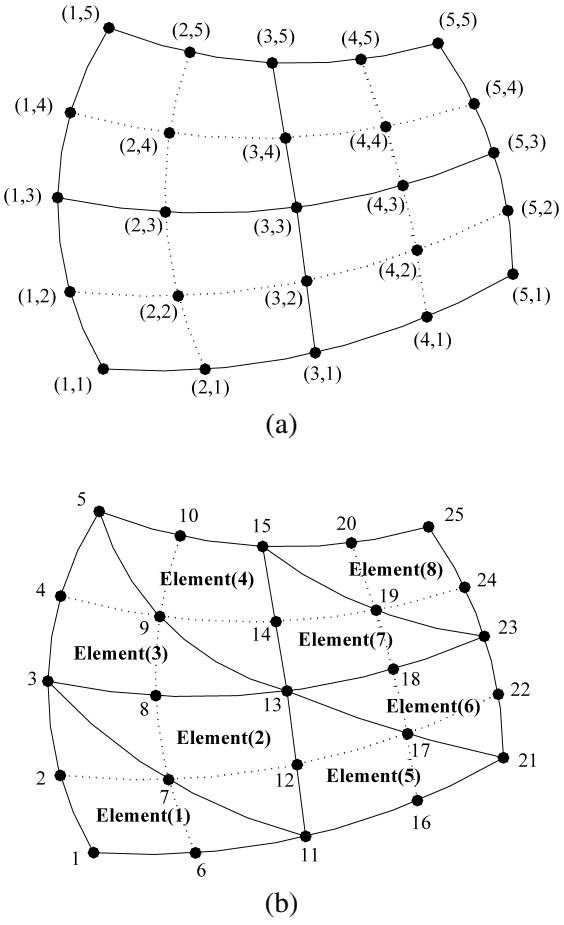

Figure 4. A transformation of numbering of nodes between FDM and FEM. (a) The numbering of grid points in FDM. (b) The nodal numbering of a 6-nodal quadratic triangular element.

Downloaded by [Siauliu University Library] at 06:59 17 February 2013

temperature, it is similar to pure metal. The fibrous preform composition is 42% alumina and 58% silica and its fiber volume fraction is 0.1. The ratio of K/μ is 9.72×10^{-10} m^3 s/kg at 90°C [13].

Figure 6 shows the flow front of the molten metal at various times during the infiltration process. Since the fibrous preform is isotropic, the fluid expands radially in the early time of the infiltration process. During this period, the governing equation (4) can be written in polar coordinates as

$$\frac{\partial^2 P}{\partial r^2} + \frac{1}{r}\frac{\partial P}{\partial r} = 0. \tag{12}$$

The boundary conditions are $P(r_\mathrm{i}) = P_\mathrm{inj}$ and $P(r_\mathrm{f}) = 0$, where r_i is the radius of the gate and r_f is the radius of the flow front. The pressure distribution in the flow

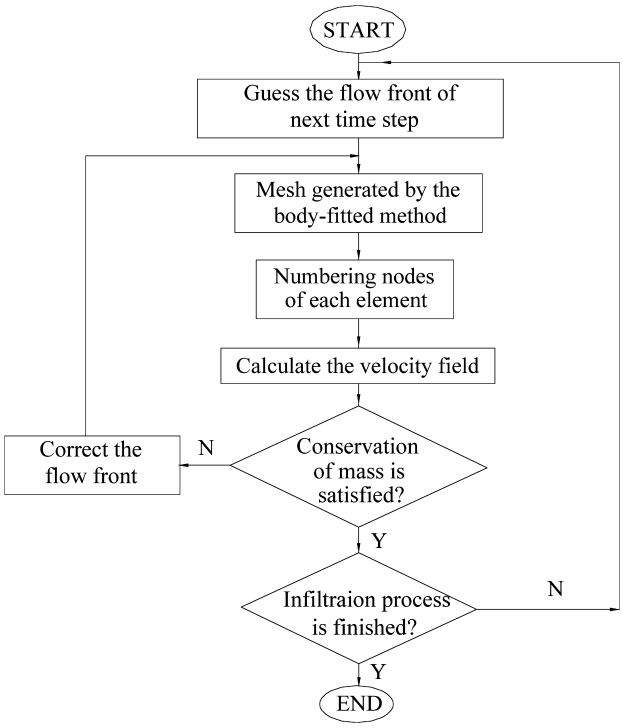

Figure 5. Flow chart of the numerical simulation.

region is

$$P(r) = P_{\text{inj}} \times (\ln r - \ln r_{\text{f}})/(\ln r_{\text{i}} - \ln r_{\text{f}}). \tag{13}$$

Substituting equation (13) into Darcy's law, the radial fluid velocity (v_{r}) is written as

$$v_{\text{r}} = \frac{\mathrm{d}r_{\text{f}}}{\mathrm{d}t} = -\frac{K}{(1-f)\mu}\left(\frac{\mathrm{d}P}{\mathrm{d}r}\right)_{r=r_{\text{f}}} = \frac{K}{(1-f)\mu}\frac{1}{r_{\text{f}}}\frac{P_{\text{inj}}}{(\ln r_{\text{f}} - \ln r_{\text{i}})}. \tag{14}$$

For the case of linearly increasing injection pressure, i.e. $P_{\text{inj}} = P_0 + P_1 t$, we can integrate equation (14) from the radius of inlet gate $r = r_{\text{i}}$ and time $t = 0$, to r and t, and the analytical relationship between flow front and time is

$$P_0 t + P_1 t^2 = \left(\frac{\mu(1-f)r_{\text{i}}^2}{K}\right) \times \left\{\frac{1}{2}\left(\frac{r_{\text{f}}}{r_{\text{i}}}\right)^2 \ln\left(\frac{r_{\text{f}}}{r_{\text{i}}}\right) + \frac{1}{4}\left(1 - \left(\frac{r_{\text{f}}}{r_{\text{i}}}\right)^2\right)\right\}. \tag{15}$$

The analytical flow front is also denoted by a dashed line as shown in Fig. 6. Apparently the analytical solution and the flow front obtained by the numerical prediction are almost identical. After the flow front contacts the side wall, the

Downloaded by [Siauliu University Library] at 06:59 17 February 2013

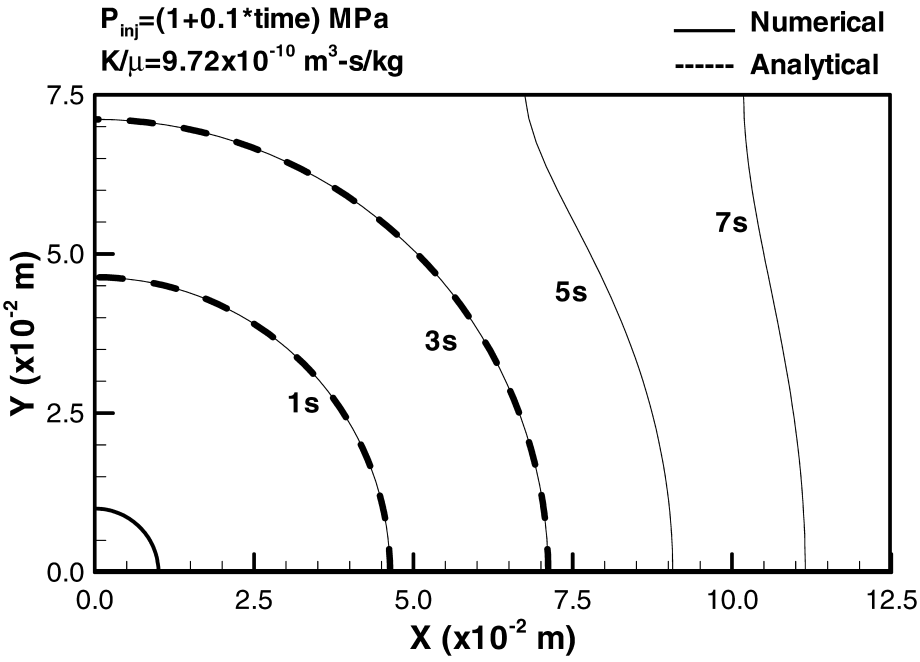

Figure 6. Motion of flow fronts of molten metal inside fibrous preform.

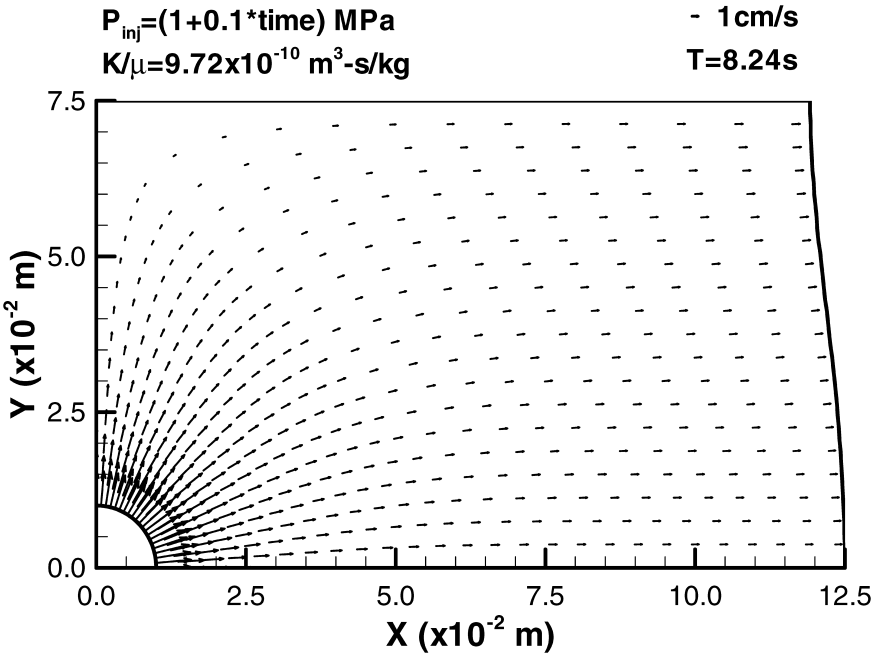

Figure 7. The velocity distribution at the infiltration time of 8.24 s.

Downloaded by [Siauliu University Library] at 06:59 17 February 2013

fluid is gradually transformed from a radial flow to a uniform flow since the flow is restricted by the side walls. The tendency of flow transformation is also observed in the velocity distribution as illustrated in Fig. 7. Figure 7 shows the velocity distribution of the molten metal in the infiltration process of the MMCs at the time of 8.24 s. Due to the viscous resistance, the fluid velocity decreases gradually from the inlet gate to the flow front. Calculation of the *Re* values during the infiltration process shows that they are about 10^{-3}. Since *Re* is much less than 1, the viscous force is significant and Darcy's law is applicable.

Figure 8 shows the exponential decrease of inlet flow rate during the infiltration process. In the early time of the infiltration process, the decrease of the inlet flow rate is sharp because the friction between the fluid and fibrous preform increases rapidly. After that, the slow decrease of the inlet flow rate is due to the fact that the driving force and viscous friction equilibrate gradually. Evidently a significant reduction in infiltration time can be achieved by using the high injection pressure. This is because the high injection pressure increases the inlet velocity.

The transient infiltration process is approximated by a series of quasi-steady-state processes in this study. A proper time increment can ensure a reasonable approximation. Through the numerical results, a suitable time constant related to

Downloaded by [Siauliu University Library] at 06:59 17 February 2013

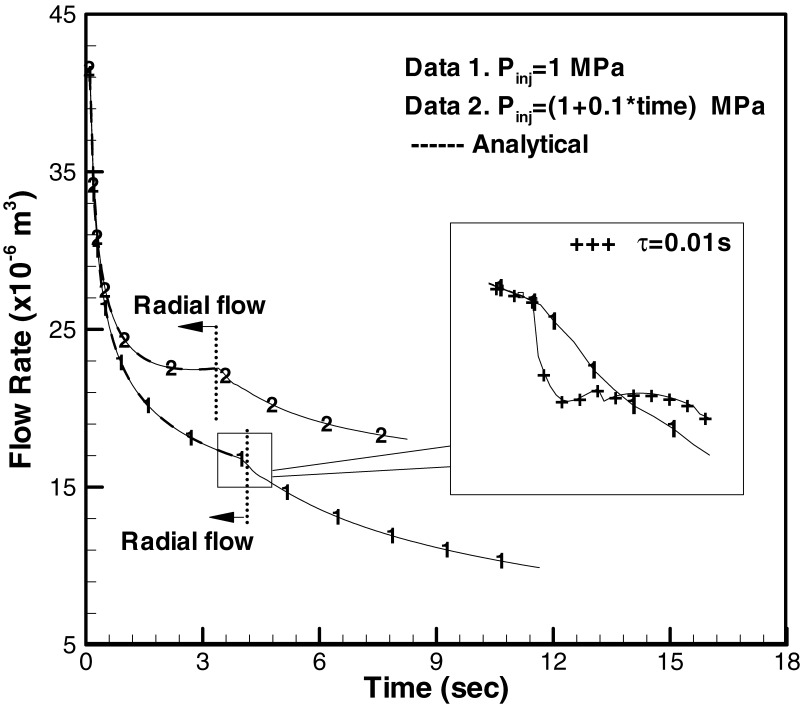

Figure 8. The variation of inlet flow rate during the infiltration process.

Table 1.
The relationship between infiltration time and injection pressure

A linearly increasing injection pressure (MPa)	Infiltration time (s)	
	Wood alloy at 90°C $K/\mu = 9.72 \times 10^{-10}$ m^3 s/kg	Aluminum at 700°C $K/\mu = 5.48 \times 10^{-10}$ m^3 s/kg
$0.5 + 0.025 * \text{time}$	16.48	22.36
$1.0 + 0.1 * \text{time}$	8.24	11.18
$1.5 + 0.225 * \text{time}$	5.49	7.45
$2.0 + 0.4 * \text{time}$	4.12	5.59
$2.5 + 0.625 * \text{time}$	3.30	4.47

Downloaded by [Siauliu University Library] at 06:59 17 February 2013

processing parameters for the infiltration process is proposed

$$\tau = \frac{\sqrt{K}}{v_c} = \frac{(1-f)\mu(W/2)\ln((W/2)/r_i)}{P_{inj} \times K^{0.5}}, \tag{16}$$

where v_c is the velocity of flow front at the contacting time when the molten metal contacts the side wall. W is the width of the mold cavity. The term on the right-hand side of equation (16) is obtained by $W/2$ substituting for r_f in equation (14). Since $K^{0.5}$ can be regarded as the characteristic length of the pore in the porous medium, the physical meaning of the time constant is the time required to advance one pore length for the fluid particle of flow front at the contacting time. If the time increment is chosen to be larger than the time constant, an excessive drop of inlet flow rate will occur about the contacting time, as shown in Fig. 8. This result agrees with that in a previously published paper [19].

The relationship between infiltration time and injection pressure is shown in Table 1. From the data a simple and practical prediction of infiltration time under the various parameters is found as follows.

$$\int_0^t \left(\frac{P_{inj}K}{\mu(1-f)}\right) dt = \text{constant}. \tag{17}$$

The physical meaning of the above equation can be considered as the volume of injection fluid being equal to that of the mold cavity. This is because the injection flow rate is directly proportional to $K \times P_{inj}/(\mu \times (1-f))$ as Darcy's law described. By the analysis, the predicted infiltration time is about 12.94 s for the case in which pure molten aluminum at 700°C ($\mu = 1.15 \times 10^{-3}$ kg/m s) and fiber volume fraction of preform equal to 0.24 ($K = 6.3 \times 10^{-13}$ m^2) are adopted under applied pressure of 1 MPa.

5. CONCLUSIONS

The aim of this study is to investigate by numerical simulation the behavior of molten metal flowing through a fibrous preform during MMC processing. To simplify the problem, the assumption of isothermally saturated fibrous preform with molten metal is adopted. The body-fitted FEM, the combination of body-fitted grid generation with the FEM, is used to solve the transient and irregular physical domains. For the case of a rectangular mold with center gate, the flow behavior of the molten metal is found to be radial in the early time of the infiltration process. After the flow front contacts the side wall, the fluid is gradually transformed to uniform flow. The inlet flow rate shows an exponential decrease during the infiltration process. A proper time increment can ensure a reasonable approximation when the infiltration process in MMCs is modeled as a series of quasi-steady-state processes. This study also provides a simple and practical prediction of infiltration time under the various parameters.

Downloaded by [Siauliu University Library] at 06:59 17 February 2013

REFERENCES

1. T. W. Chou, A. Kelly and A. Okura, Fiber-reinforced metal-matrix composites, *Composites* **16**, 187–206 (1985).
2. E. Lacoste, M. Danis, F. Girot and J. M. Quenisset, Numerical simulation of the injection moulding of thin parts by liquid metal infiltration of fibrous preforms, *Mat. Sci. Eng. A-Struct*. **135**, 45–49 (1991).
3. V. J. Michaud and A. Mortensen, Infiltration of fiber preforms by a binary alloy: Part II. Further theory and experiments, *Metall. Trans. A* **23**, 2263–2280 (1992).
4. A. Mortensen and L. Jin, Solidification processing of metal matrix composites, *Int. Mater. Rev.* **37**, 101–128 (1992).
5. R. Asthana, P. K. Rohatgi and S. Tewari, Infiltration processing of metal-matrix composites: a review, *Processing Adv. Mater*. **2**, 1–17 (1992).
6. A. Mortensen, L. J. Masur, J. A. Cornie and M. C. Flemings, Infiltration of fibrous preforms by a pure metal: Part I. Theory, *Metall. Trans. A* **20**, 2535–2547 (1989).
7. V. J. Michaud, L. M. Comption and A. Mortensen, Capillarity in isothermal infiltration of alumina fiber preforms with aluminum, *Metall. Mater. Trans. A* **25**, 2145–2152 (1994).
8. L. J. Masur, A. Mortensen, J. A. Cornie and M. C. Flemings, Infiltration of fibrous preforms by a pure metal: Part II. Experiment, *Metall. Trans. A* **20**, 2549–2557 (1989).
9. A. Mortensen and T. Wong, Infiltration of fibrous preforms by a pure metal: Part III. Capillary phenomena, *Metall. Trans. A* **21**, 2257–2263 (1990).
10. A. Mortensen and V. J. Michaud, Infiltration of fibrous preforms by a binary alloy: Part I. Theory, *Metall. Trans. A* **21**, 2059–2072 (1990).
11. J. L. Sommer and A. Mortensen, Forced unidirectional infiltration of deformable porous media, *J. Fluid Mech*. **311**, 193–217 (1996).
12. V. J. Michaud, J. L. Sommer and A. Mortensen, Infiltration of fibrous preforms by a pure metal: Part V. Influence of preform compressibility, *Metall. Mater. Trans. A* **30**, 471–482 (1999).
13. M. Aboulfatah, M. Danis and E. Lacoste, Mobility of molten metal through a fibrous preform during MMC processing, *J. Mater. Syn. Process*. **5**, 459–466 (1997).
14. Z. Xia, Y. Zhou, Z. Mao and B. Shang, Fabrication of fiber-reinforced metal matrix composites by variable pressure infiltration, *Metall. Mater. Trans. B* **23**, 295–302 (1992).

15. E. Lacoste, M. Aboulfatah, M. Danis and F. Girot, Numerical simulation of the infiltration of fibrous preforms by a pure metal, *Metall. Mater. Trans. A* **24**, 2667–2678 (1993).
16. X. Tong and J. A. Khan, Infiltration and solidification/remelting of a pure metal, *J. Heat Transfer* **118**, 173–180 (1996).
17. D. K. Biswas, J. E. Gatica and S. N. Tewari, Dynamic analysis of unidirectional pressure infiltration of porous preforms by pure metals, *Metall. Mater. Trans. A* **29**, 377–385 (1998).
18. T. Dopler, A. Modaressi and V. Michaud, Simulation of metal-matrix composite isothermal infiltration processing, *Metall. Mater. Trans. B* **31**, 225–234 (2000).
19. C. J. Wu and L. W. Hourng, Permeable boundary condition for numerical simulation in resin transfer molding, *Polym. Eng. Sci.* **35**, 1272–1281 (1995).
20. D. S. Burnett, *Finite Element Analysis*. Addison-Wesley Publishing Company, Singapore (1988).
21. P. D. Thomas and J. F. Middlecoff, Direct control of the grid point distribution in meshes generated by elliptic equation, *AIAA J*. **18**, 652–656 (1980).

Downloaded by [Siauliu University Library] at 06:59 17 February 2013